

# Prompt-Tuning SAM: From Generalist to Specialist with only 2,048 Parameters and 16 Training Images

Tristan Piater Björn Barz Alexander Freytag  
Carl Zeiss AG, Germany

tristan.piater@zeiss.com, bjoern.barz@zeiss.com, alexander.freytag@zeiss.com

## Abstract

The Segment Anything Model (SAM) is widely used for segmenting a diverse range of objects in natural images from simple user prompts like points or bounding boxes. However, SAM’s performance decreases substantially when applied to non-natural domains like microscopic imaging. Furthermore, due to SAM’s interactive design, it requires a precise prompt for each image and object, which is unfeasible in many automated biomedical applications. Previous solutions adapt SAM by training millions of parameters via fine-tuning large parts of the model or of adapter layers. In contrast, we show that as little as 2,048 additional parameters are sufficient for turning SAM into a use-case specialist for a certain downstream task. Our novel PTSAM (prompt-tuned SAM) method uses prompt-tuning, a parameter-efficient fine-tuning technique, to adapt SAM for a specific task. We validate the performance of our approach on multiple microscopic and one medical dataset. Our results show that prompt-tuning only SAM’s mask decoder already leads to a performance on-par with state-of-the-art techniques while requiring roughly 2,000x less trainable parameters. For addressing domain gaps, we find that additionally prompt-tuning SAM’s image encoder is beneficial, further improving segmentation accuracy by up to 18% over state-of-the-art results. Since PTSAM can be reliably trained with as little as 16 annotated images, we find it particularly helpful for applications with limited training data and domain shifts.

## 1. Introduction

Biological research relies strongly on high-throughput experiments. Consequently, high amounts of recorded data need to be reliably analyzed at scale [2, 3, 48–50]. It is therefore no surprise that automated image analysis techniques are of utmost importance. One important technique is semantic segmentation, which enables a broad range of solutions, like automatic calculation of cell mass [2, 49],

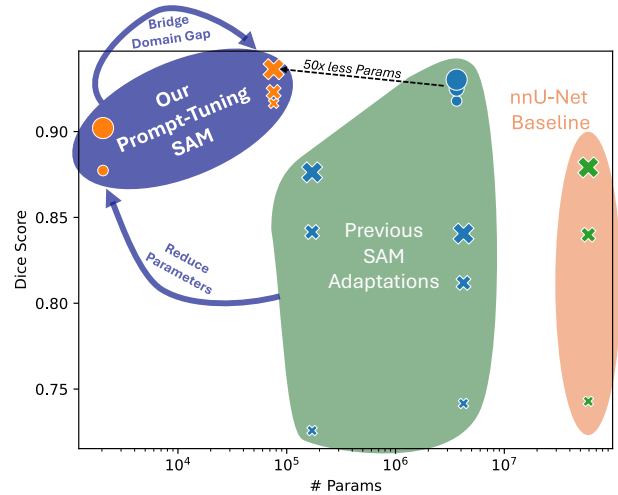


Figure 1. Comparison of Prompt-Tuning SAM (ours) to other techniques for adapting SAM, as well as nnU-Net as the de-facto standard. Circles indicate adapting the mask decoder only, while crosses indicate additional adaptation of the image encoder. Marker sizes correlate with the number of training images.

comparison of organoid volumes [48], and detection of mitotic cells [3]. Because applications can differ strongly, *e.g.*, in the required microscopic imaging modality [50], or in the targets to segment, each application currently requires a separate model that is explicitly trained for this specific task. However, training such a specialist model is expensive, requiring computational resources, annotated data, and time of machine learning experts. All three aspects are usually rare resources in microscopy image analysis facilities.

In contrast to such specialized models, the recent success of large-scale unsupervised pre-training especially for transformer architectures started a shift towards generalist models [1, 7, 55]. These so-called foundation models [6], enabled by self-supervised pre-training without being trained for only one specific use case, have advanced zero- and few-shot generalization [7] to solve tasks outside of their training domain. After having started in the language

domain, benefits of foundation models were explored in the vision domain as well [13, 21, 45]. Consequently, vision foundation models (VFM) were developed across many domains, *e.g.*, RetFound by Neto and Regattieri [44] enabling fast training of *any* retina analysis solutions, DepthAnything by Yang et al. [60] performs depth estimation for *any* scene, or UniverSeg by Butoi et al. [8], which performs in-context segmentation of *any* medical object. In the following, we will focus on another popular VFM: the Segment Anything Model (SAM) by Kirillov et al. [31], which enabled interactive segmentation of *any* natural-scene object.

SAM can be applied to a wide range of tasks with impressive zero-shot results. To achieve this performance, SAM was trained on SA-1B [31], a huge segmentation database consisting of one billion of masks. However, as SA-1B covers only natural images, it can not be expected a-priori that SAM generalizes beyond natural images. In fact, it has been shown that SAM’s segmentation performance significantly drops when applied in non-natural image domains like agriculture, medicine and microscopy [4, 10, 27, 29, 52]. Furthermore, SAM requires user prompts for each image and instance. This interactive design renders SAM unsuitable for high-throughput experiments, where large quantities of objects and images need to be segmented [4, 52]. However, it appears promising to build a use-case specialist out of SAM, thereby keeping its knowledge while reduce the training costs and the required amount of labelled training data for one specific task.

This idea has been investigated extensively [4, 27, 43, 54], resulting in different techniques for adapting SAM for bridging the domain gap between the pre-training and target domain or to remove the need for user-defined prompts for each image. Inspired by recent developments and their remaining short-comings, we propose prompt-tuning SAM, or short PTSAM, which leverages prompt-tuning techniques [30, 34, 36] to fine-tune SAM’s image encoder and mask decoder in an extremely parameter-efficient manner, thereby enabling robust training in data-limited scenarios and memory-efficient model distributions. Our experiments on microscopic and medical imaging datasets underpin the following contributions of our approach:

1. PTSAM allows for obtaining a specialist model with only 2,048 trainable parameters that is on par with state-of-the-art microscopic image segmentation models.
2. We find that additionally adapting the image encoder with PTSAM is beneficial for bridging the domain gap and further improves performance by up to 21%.
3. PTSAM provides consistent performance even when reducing the number of training images from 64 to 16, leading to useful segmentation results where other methods that adapt the image encoder are prone to overfitting in a limited-data regime.

These findings are visualized in Figure 1.

## 2. Related Work

### 2.1. Image Segmentation

Without any doubt, the U-Net CNN architecture by Ronneberger et al. [46] is the de-facto standard for biomedical image segmentation. A pivotal development of U-Net is nnU-Net [26], which provides automated configurations for hyperparameters of model and training, thereby enabling the development of solutions for segmenting medical images without advanced machine learning expertise.

CellSeg [32], on the other hand, pretrains a Mask R-CNN [20] on nucleus segmentation tasks, to get an easy to adapt cell segmentation model. Other approaches [16, 18, 63] extend convolutional neural networks with transformer layers [55] to improve the performance for biomedical image segmentation. However, these models need to be trained for each task individually.

### 2.2. Promptable Vision Foundation Models

In contrast to task-specific specialist models, foundation models [6] provide the capability of being adaptable to tasks outside of their training domain. One way for adaptation is prompting [1, 7], *e.g.*, as well-known from language models like the GPT series [1, 7]. Following this success, transformers and self-supervised large-scale training were adapted for the vision domain [13, 21, 45]. A milestone of this research direction is the Segment Anything Model (SAM) [31], a foundation model for image segmentation. Based on user prompts such as point coordinates or boxes, SAM adapts from segment-anything generalist to highly accurate instance-specific specialist. However, needed promptability hinders applications in fully-automated workflows.

### 2.3. Parameter-Efficient Fine-Tuning (PEFT)

Historically, deep learning specialist models were either trained from scratch [26] or adapted through fine-tuning pre-trained parameters [19]. However, for adapting a foundation model via training towards a specific downstream task, full fine-tuning is often not feasible, especially because of the high computational requirements for training these models. Therefore, parameter-efficient fine-tuning (PEFT) methods have been developed [15, 58, 59], which update only a fraction of the trainable parameters or a small re-parametrization of the model. A common PEFT approach is to select only a certain set of parameters to train. Early approaches trained the last (few) layers of a network [12, 23, 39], where recently, the set of these learnable parameters shifted towards bias terms [9], normalization layers [5], or weights in attention operations [51].

In contrast to these selective fine-tuning methods, feature adapters [22, 38, 47] introduce new parameters in the model which are trained during training while the original

network is kept frozen. Similarly popular is low-rank adaptation (LoRA) by Hu et al. [24]. LoRA freezes MLP layers and approximates their updates with a learnable low-rank matrix decomposition. The lower the rank of these matrices, the lower the number of trainable parameters. QLoRA [11] further optimizes LoRA by quantizing the original weights to 4 bits. A final notable technique is input tuning, also known as visual prompt tuning, *e.g.*, by Jia et al. [30], which adds new trainable parameters not directly in the model, but at the image space. All these methods allow to adapt an existing model to a new task while keeping the overall input-output relation unchanged. Thus, while applying PEFT to SAM would enable adapting SAM to a new domain [4, 62], they do not overcome SAM’s needed promptability.

## 2.4. Adapting SAM

Different PEFT methods were developed for adapting SAM to a new domain. In combination with removing the need of manual prompts, SAM becomes capable of automatically generating masks for certain tasks. One approach to remove SAM’s interactive design is to simulate user prompts. Wu et al. [57] trained a logistic regression to predict foreground pixels on the image embeddings. From this binary map, point and bounding box prompts are calculated, which are fed to the prompt encoder. Methods for the microscopy domain [4, 27, 43] use more complex autoprompting modules such as UNETR, DETR, and U-Net [17, 46, 56]. Additionally, these methods train further components of SAM to bridge the domain gap. However, they still work with SAM’s user prompts, which are obsolete when performing automatic segmentation. Furthermore, to perform semantic segmentation, each instance needs to be segmented individually, which is inefficient for a large number of instances.

In contrast, other SAM adaptations fine-tune the mask decoder to solve a specific task. Hu et al. [25] train different kinds of segmentation heads on top of SAM’s image embeddings. Their approach called AutoSAM uses SAM’s mask decoder architecture and fully trains it for a specific task. SAMed [62] additionally applies LoRA fine-tuning to the image encoder. In the microscopic domain, SAM-Cell [54] fully fine-tunes the mask decoder as well, but also fully trains the image encoder. While the number of parameters inside the mask decoder is manageable, it is still high enough to benefit from the use of PEFT techniques, which these works did not explore.

CellSeg1 [64] heavily reduces the number of trainable parameters by using LoRA to parameter-efficiently adapt the mask decoder and the image encoder instead of fine-tuning them fully. Hence, CellSeg1 accurately segments cells after training on just one input image. However, to do that, users still need to provide prompts, *i.e.*, it cannot segment objects fully automatically.

Our approach combines the advantages of PEFT and au-

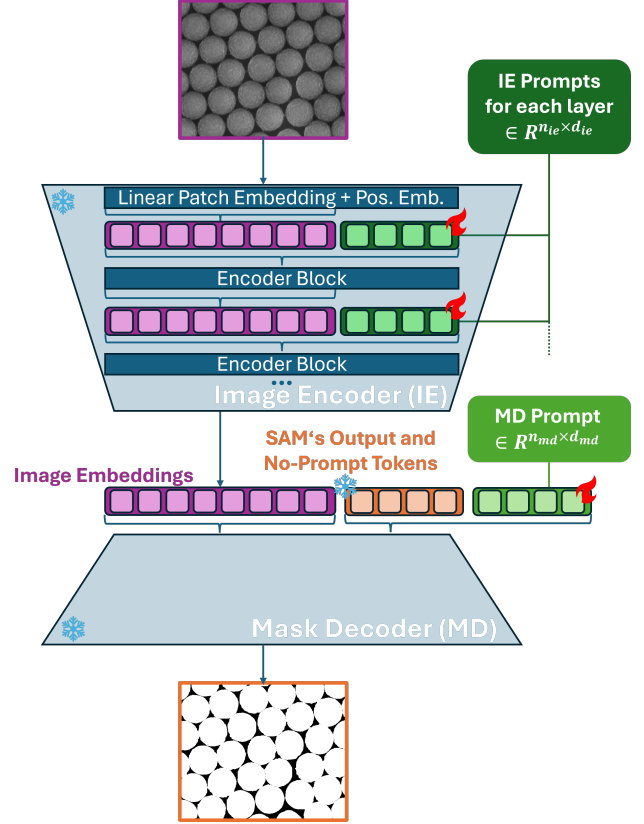


Figure 2. Overview of our PTSAM approach. We remove the prompt-encoder from the SAM architecture [31], which we keep frozen. Instead, we add learnable prompt parameters (green) into the mask decoder for becoming a use-case specialist and into the each layer of the image encoder to address domain shifts.

tomatic segmentation, solving the issues of prompt generation and domain shift at once. Instead of using LoRA such as most prior works, we adopt prompt tuning by Jia et al. [30] for adapting the mask decoder and image encoder, which is even more parameter-efficient.

## 3. Method

In the following, we first briefly describe the relevant parts of SAM’s original architecture in Sec. 3.1 and then introduce our PTSAM approach for turning SAM into a specialist with few annotated examples in Sec. 3.2.

### 3.1. SAM

As nicely visualized in Figure 4 of [31], SAM consists of three main components: the image encoder, the prompt encoder, and the mask decoder. The image encoder of SAM is a Vision Transformer [13], pre-trained with a masked auto-encoder (MAE) criterion [21]. It takes input images with a size of  $1,024 \text{ px} \times 1,024 \text{ px}$  and predicts an image feature map of resolution  $64 \text{ px} \times 64 \text{ px}$  with 256 feature channels

per cell. To process high resolution input images, the design for the image encoder is adopted from the work by Li et al. [37] for vision transformers as object detection backbones. In particular, it uses a  $14 \times 14$  windowed attention and four global attention blocks, which are spaced equally throughout the layers of the transformer.

The prompt encoder embeds different types of user prompts, which are used to describe the desired object. Masks as dense prompts are added to the image embeddings through convolutional operations, while sparse prompts like points and boxes are fed to the mask decoder. These sparse prompts are encoded with a combination of positional and learned embeddings. The positional embeddings encode the coordinates of the point or the corners of the bounding box. The learned embeddings provide information about the type of prompt, *i.e.*, differentiating between the corners of the bounding box or whether the point belongs to foreground or background. If no user prompts are provided, a no-prompt-embedding is used instead.

SAM’s mask decoder predicts the segmentation map based on two input streams: the image embeddings and a token stream. The latter one consists of embeddings of the sparse user prompts and learned output tokens. Both streams are the input to a two-layer transformer, which applies self attention to the token stream and cross attention from the token to the image stream and vice versa. Finally, the image embeddings are upsampled with a transposed convolutional neural network and the output tokens are projected through a multi-layer perceptron. The segmentation map is then calculated as a pixel-wise dot product of both results. To account for prompt ambiguity, three output tokens are used to predict three output masks, one for object, part, and subpart. A fourth IoU token is used for predicting which of these three outputs is the desired one.

### 3.2. PTSAM

Adapting SAM from a promptable generalist to a use-case specialist requires two things: i) an automatic generation of segmentation maps without user prompts and ii) an adaptation to a novel domain. We propose to address both requirements with the same underlying base technique: by transferring the idea of visual prompt-tuning [30] to SAM, giving rise to the name PTSAM. Our resulting specialist adaptation of SAM to PTSAM is visualized in Fig. 2.

PTSAM keeps the original SAM architecture frozen and only trains inserted prompts. Specifically, we add trainable prompt parameters into SAM’s mask decoder, thereby replacing the interactive segment *anything* aspect of SAM with a trainable segment *this specific task* ability. Hence, SAM’s prompt encoder becomes obsolete and, therefore, we remove it from the architecture.

In turn, we extend the token-stream used as input for the mask decoder with  $n_{\text{md}}$  trainable prompts  $\mathbf{p}_{\text{md}} \in \mathbb{R}^{n_{\text{md}} \times d_{\text{md}}}$ ,

where the dimension of the mask decoder is  $d_{\text{md}} = 256$ . However, to maintain the pretrained behavior of SAM, we keep the no-prompt embedding in addition to all output tokens. We only use the first of the three resulting segmentation maps as output. During training, the added prompts are learned to segment the object of interest. In contrast to the user prompts, which only encode positional information, our prompts belong to the latent prompt embedding space and can hence be more expressive.

For further addressing any potential mismatch between the pretraining and target image domain, we additionally insert prompts into the image encoder using the deep visual prompt-tuning (VPT) method introduced by Jia et al. [30]. Hence, instead of extending the inputs of the first layer only, we prompt each layer  $l$  of the vision transformer with  $n_{\text{ie}}$  learnable prompts  $\mathbf{p}_{\text{ie}}^{(l)} \in \mathbb{R}^{n_{\text{ie}} \times d_{\text{ie}}}$ , with  $d_{\text{ie}}$  being the dimension of the ViT. Due to the windowed attention of the image encoder, we insert the same prompts to each of the  $14 \times 14$  windows at a certain layer. During training, we keep all of SAM’s weights frozen, and learn only the inserted continuous prompt vectors  $\mathbf{p}_{\text{md}}$  and  $\mathbf{p}_{\text{ie}}^{(l)}$ . Thereby, user-prompt-free segmentation and domain shift can be tackled, while needing only a small number of parameters to train.

## 4. Experiments

We evaluate the effectiveness of PTSAM for transforming SAM into a use-case specialist on multiple application-relevant datasets, specifically on three microscopic and one medical image segmentation task. The performance is compared with state-of-the-art adaption techniques for SAM, as well as non-promptable segmentation standards. The choice of datasets allows for assessing the necessity of addressing the domain shift from natural to non-natural images.

### 4.1. Experimental Setup

#### 4.1.1. Methods

We compare our PTSAM approach with two other methods for adapting SAM to specific downstream tasks. Specifically known in the microscopy image analysis domain is CellSeg1 by Zhou et al. [64], which tunes the image encoder and mask decoder with LoRA [24]. This method preserves the promptability of the model, making it not immediately applicable as use-case specialist. Therefore, we modify CellSeg1 and use SAM’s no-prompt-embeddings during training, enabling CellSeg1 to automatically generate masks. Similarly popular is SAMCell [54], which however fine-tunes the entire image encoder. When replacing full fine-tuning with LoRA training, SAMCell becomes a parameter-efficient adaptation technique, which is identical to a method known as SAMed [62] in the medical domain. We compare PTSAM against SAMed for a fair comparison.

We are specifically interested in analyzing the effects of



Method	IE	MD	# Param
PTSAM (Ours)	-	PT	2,048
	PT	PT	75,776
CellSeg1 [64]	-	LoRA	23,552
	LoRA	LoRA	171,008
AutoSAM [25]	-	Fully	3,645,344
SAMed [62]	LoRA	Fully	4,212,016
nnU-Net [26]	-	-	59,177,872

Table 1. Methods overview with indications about the technique to train the image encoder (IE) and mask decoder (MD), and the corresponding number of trainable parameters.

training only the mask decoder (for making SAM a specialist) or additionally the image encoder (for addressing the domain shift). Therefore, we analyze all SAM adaptations in two settings: once with the parameter efficient fine-tuning of the image encoder, and once where we keep it frozen. SAMCell’s architecture with a frozen image encoder is the same as AutoSAM [25].

In addition to these SAM adaptations, we use nnU-Net [26] as a baseline for training a specialist from scratch.

We give a summarizing overview on all these methods in Tab. 1, further highlighting which parts are adjustable and the resulting number of trainable parameters.

#### 4.1.2. Datasets

We evaluate all methods on three datasets from the life-science microscopy domain as well as one medical image segmentation dataset. Lifescience datasets were selected to cover different imaging modalities as well as different target applications. The OrganoidBasic dataset [33, 53] was captured with bright-field microscopy and contains organoids to be segmented. As complementary modality, the EMParticles dataset [61] contains electron-microscopical images with varying targets to be segmented. In addition, the LiveCell dataset [14] shows living cells in phase contrast images. Finally, KvasirSEG [28] serves as a non-microscopy dataset, covering gastrointestinal polyp images as a representative scenario for medical imaging applications. We include it in our experiments to analyze which approaches generalize beyond microscopy scenarios to other imaging and application domains.

Since annotated samples are expensive especially in these applications, the number of required images to train a specialist segmentation model should be as low as possible. Hence, we evaluate each method in three scenarios with random subsets of 16, 32, or 64 annotated training samples. Across these scenarios, we keep consistent test sets with 20% of all samples to allow for meaningful comparisons.

#### 4.1.3. Hyperparameters

The scarcity of annotated training data poses another problem for real-world use cases: thorough hyperparameter op-

timization becomes infeasible. Hence, we base our hyperparameter selection on common practices from the literature. By keeping the setup consistent throughout different runs, we furthermore increase comparability.

For all SAM-based methods, we use the ViT-b variant as the image encoder with the original SAM weights. These weights are also used on the medical dataset instead of domain-specialized weights such as those from MedSAM [42] because Li and Rajpurkar [35] found better performance when fine-tuning SAM’s original weights to a new task. We optimize the learning rate individually for each method on a heldout dataset. For our PTSAM method, we found a learning rate of 0.05 to be optimal when keeping the image encoder frozen. Training the image encoder in addition reaches best metrics with a learning rate of 0.01.

Method-specific hyper-parameters of other approaches, *e.g.*, the rank in LoRA, are set to the values proposed in the original papers. For our PTSAM model, we found in preliminary experiments that increasing the number of image encoder and mask decoder prompts beyond 8 does not lead to further improvements (see Sec. 4.3). Hence, we set  $n_{md} = n_{ie} = 8$ . With the mask decoder dimension  $d_{md} = 256$ , we have  $256 \cdot 8 = 2,048$  trainable parameters for the mask decoder. The ViT-b image encoder consists of 12 layers, each having a dimension of  $d_{ie} = 768$ , resulting in  $12 \cdot 768 \cdot 8 = 73,728$  trainable parameters.

The well-tested setup used by nnU-Net serves as a reference for other training parameters. Specifically, we fix the number of epochs to 1,000 and the number of optimization steps in each epoch to 20. Thereby, the number of training steps is independent of the dataset size, which allows conclusions about the relation of dataset size and method performance. Throughout the training, we reduce the initial learning rate with cosine annealing [40]. To prevent overfitting in our low-data regime, we apply heavy data augmentations. We combine the setups from [25, 26, 62, 64], *i.e.*, we apply randomized usage of rotation, cropping, elastic transformations, flips, Gaussian noise, and changes of Gamma, brightness, and contrast. For the choice of the optimizer and loss, we follow other SAM adaptations [25, 27, 54, 62, 64] and use AdamW [41] as the optimizer and a weighted sum of cross-entropy loss and Dice loss. Following Zhang and Liu [62], we weight these two losses with 0.2 and 0.8, respectively. Finally, we set the batch size to two, which enables training SAMs image encoder even on consumer-grade hardware.

## 4.2. Results

We report all results with mean and standard deviation of Dice scores aggregated over three random splits per dataset in Tab. 2.

Dataset	# Imgs	Frozen IE			Trained IE			nnU-Net
		PTSAM	CellSeg1	AutoSAM	PTSAM	CellSeg1	SAMed	
EMParticles	16	87.7 $\pm$ 1.4	88.1 $\pm$ 2.8	<b>91.8<math>\pm</math>3.0</b>	91.7 $\pm$ 3.7	72.6 $\pm$ 1.4	74.2 $\pm$ 3.6	74.3 $\pm$ 2.2
	32	90.0 $\pm$ 2.2	90.1 $\pm$ 3.1	<b>92.5<math>\pm</math>3.0</b>	92.3 $\pm$ 2.5	84.1 $\pm$ 1.1	81.2 $\pm$ 3.2	84.0 $\pm$ 2.9
	64	90.2 $\pm$ 1.7	89.9 $\pm$ 3.1	93.0 $\pm$ 2.4	<b>93.6<math>\pm</math>2.7</b>	87.6 $\pm$ 3.5	84.1 $\pm$ 2.1	87.9 $\pm$ 3.8
LiveCell	16	86.0 $\pm$ 0.5	86.5 $\pm$ 0.2	88.0 $\pm$ 0.2	<b>89.6<math>\pm</math>0.4</b>	89.2 $\pm$ 0.3	88.1 $\pm$ 0.3	88.5 $\pm$ 1.4
	32	86.4 $\pm$ 0.4	86.8 $\pm$ 0.5	88.7 $\pm$ 0.4	<b>90.2<math>\pm</math>0.4</b>	89.1 $\pm$ 0.5	88.4 $\pm$ 0.2	89.5 $\pm$ 1.3
	64	86.4 $\pm$ 0.3	87.5 $\pm$ 0.3	89.4 $\pm$ 0.2	<b>90.5<math>\pm</math>0.2</b>	90.1 $\pm$ 0.2	88.9 $\pm$ 0.3	<b>90.5<math>\pm</math>0.3</b>
OrganoidBasic	16	89.4 $\pm$ 0.5	90.2 $\pm$ 0.5	90.9 $\pm$ 0.4	<b>91.6<math>\pm</math>0.4</b>	90.3 $\pm$ 1.2	90.0 $\pm$ 0.8	<b>91.6<math>\pm</math>0.5</b>
	32	89.9 $\pm$ 0.5	90.6 $\pm$ 0.4	91.2 $\pm$ 0.3	<b>91.8<math>\pm</math>0.5</b>	90.8 $\pm$ 0.3	90.7 $\pm$ 0.5	91.7 $\pm$ 0.3
	64	89.9 $\pm$ 0.8	90.7 $\pm$ 0.5	91.5 $\pm$ 0.5	<b>92.0<math>\pm</math>0.6</b>	91.3 $\pm$ 0.8	91.0 $\pm$ 0.8	91.9 $\pm$ 0.8
KvasirSEG	16	63.9 $\pm$ 7.4	61.5 $\pm$ 5.9	60.2 $\pm$ 4.7	<b>75.7<math>\pm</math>5.5</b>	52.4 $\pm$ 2.3	45.1 $\pm$ 2.7	50.0 $\pm$ 5.1
	32	66.1 $\pm$ 3.2	65.2 $\pm$ 2.7	63.1 $\pm$ 8.1	<b>80.2<math>\pm</math>2.7</b>	56.8 $\pm$ 2.8	48.4 $\pm$ 2.9	62.6 $\pm$ 7.3
	64	69.4 $\pm$ 3.6	69.3 $\pm$ 3.1	70.3 $\pm$ 2.3	<b>84.1<math>\pm</math>3.8</b>	64.6 $\pm$ 1.6	52.8 $\pm$ 2.6	71.8 $\pm$ 3.0

Table 2. Dice scores in percent of all experiments. We report mean and standard deviation obtained from three runs. Higher values are better. The method with best mean score on each dataset is highlighted in **green**. The bold PTSAM method is ours.

#### 4.2.1. Lifescience Microscopy Image Segmentation

On the microscopic datasets EMLParticles, LiveCell, and OrganoidBasic, our PTSAM with a trained image encoder reaches the highest Dice scores in the clear majority of cases. Noteworthy, training the image encoder with PTSAM consistently improves results on all datasets over prompt-tuning only the mask-decoder. In contrast, we observe on the EMLParticles dataset that all other methods which adapt image encoders (including nnU-Net) fail to learn reliable segmentation models, most strongly visible with only 16 training images. Given the large parameter counts, we attribute this behavior to overfitting.

When comparing the methods with a frozen image encoder, we initially observe that PTSAM leads to lower Dice scores than CellSeg1 and AutoSAM. On a second view, however, we see that statistical significance of differences is often weak (as indicated by the relatively large standard deviations), and that in addition, the number of needed parameters for both methods is substantially larger. Hence, we conclude that PTSAM allows training of microscopy specialists which are similarly accurate as other methods while needing only 2,048 parameters to train.

#### 4.2.2. Medical Image Segmentation

On KvasirSEG, both PTSAM versions outperform their competitors in nearly all cases. On closer look, we observe that all methods with a frozen image encoder (left column in Tab. 2) perform comparably. This finding is consistent with the previously discussed results on the microscopy datasets, and it is indeed surprising, given that our PTSAM uses >10x less trainable parameters than the other methods. When adapting the image encoder to account for the domain gap, however, PTSAM alone clearly benefits, while

CellSeg1, SAMed, and even nnU-Net obtain substantially worse results than with a frozen image encoder. We again attribute the superior results of this larger PTSAM version to its robustness against overfitting.

#### 4.2.3. The Effect of Image Encoder Adaptation

We have already seen on the medical dataset KvasirSEG that other techniques which adapt the image encoder lead to inferior segmentation performance compared to their mask-decoder-only adapted versions. Experiments on the EMLParticles dataset came to a similar conclusion. We further analyze this observation by visualizing in Fig. 3 the difference of the Dice score between models with and without an adapted image encoder. Higher values indicate increased performance when training the image encoder. In contrast to other SAM adaptations, PTSAM does not experience a performance decrease when tuning the image encoder. Instead, we see consistent benefits of PTSAM with trained image encoder across all datasets. Interestingly, benefits are largest on medical data (shown in **orange**). We assume that this improvement can be attributed to the application modality: objects in KvasirSEG do not have clear edges, which is uncommon in SAM’s original training domain [25, 42].

#### 4.2.4. The Effect of Less Training Data

In real-world scenarios, even collecting just 64 images for a single use case can be intractable. We therefore visualize the impact that a reduction of the training dataset from 64 to 16 samples has on the resulting segmentation accuracy of each method in Fig. 4. Results are obtained by averaging results from Tab. 2 of all four datasets. We observe that when training without image encoder adaptation (**blue**), segmentation accuracy drops only slightly by  $\sim 2\%$  when reducing the training size by 4x. Note again that nnU-Net has no blue

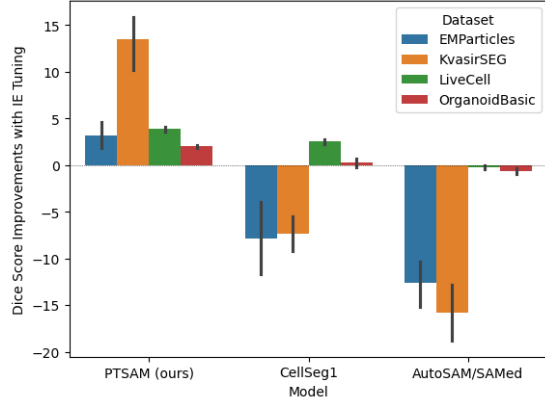


Figure 3. Comparing improvements of different methods when additionally tuning the image encoder. Higher values show that tuning the image encoder is beneficial.

bar since the image encoder is always trained from scratch. However, when the image encoder is also adapted, we observe stronger drop in performance for the previous SAM adaptation methods of  $\sim 4-6\%$  Dice score. nnU-Net struggles with a too small training set as well, leading even to an average drop of  $\sim 8\%$  Dice score. From all analyzed methods, our PTSAM is the least affected from small training set sizes, making it well-suited for few-shot scenarios.

#### 4.2.5. Qualitative Results

We show random samples and the predictions of our PTSAM approach with frozen and tuned image encoder, AutoSAM as second best method, and nnU-Net as classical baseline in Fig. 6. For better comparison, we highlight false negatives in orange and false positives in red. The segmentation maps on the OrganoidBasic dataset are in all cases very promising and similar. Noticeably, both methods with a frozen image encoder predict the same false positive object at the upper border of the image, while the fully trained PTSAM and nnU-Net cannot find an organoid in the upper-left part of the image. On the EMParticles dataset, the resulting segmentation maps differ. PTSAM with a frozen image encoder predicts most particles, while not being accurate on the boundaries. With a tuned image encoder, the particles are segmented well but with some missing, which have a lower contrast in the input image. AutoSAM predicts these but shows problems on the borders of the particles. In contrast, nnU-Net struggles a lot with the large number of particles. On the sample from the LiveCell dataset, all methods behave similarly. They predict the same false-positive structures, and they miss borders of individual cells within cell groups. PTSAM without image encoder tuning also predicts multiple wrong small structures throughout the whole slice. On the medical KvasirSEG dataset, both PTSAM methods yield the most accurate segmentations. PT-

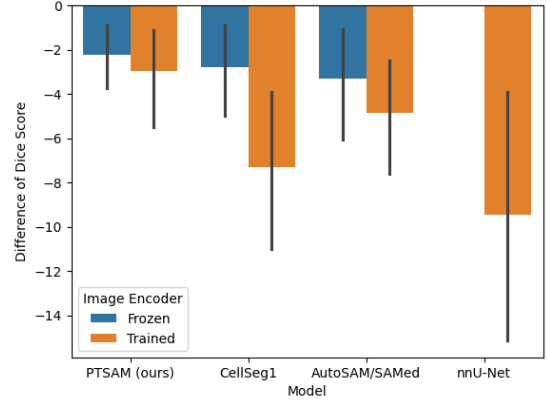


Figure 4. Performance decrease of the methods, when training with 16 instead of 64 images. Lower values indicate, that the method requires more training data.

SAM with a fixed image encoder leads to a patchy shape, while tuning the encoder results in a more consistent segmentation. AutoSAM only segments the lower part of the polyp and the prediction of nnU-Net is very off again.

#### 4.3. Ablation on Number of Prompt Parameters

Our PTSAM method has two architecture-specific hyperparameters: the number of prompts for the mask decoder  $n_{md}$  and the image encoder  $n_{ie}$ . As described already, all results in Tab. 2 were obtained by optimizing hyperparameters initially on a held-out dataset and then keeping them fixed for all remaining experiments. The results of our initial ablation experiments are shown in Fig. 5. We observe that with a frozen image encoder, increasing the number of mask decoder prompts until  $n_{md} = 8$  leads to higher Dice scores, but reaches a plateau afterwards. We then fix the number of mask decoder prompts to 8 and additionally prompt-tune

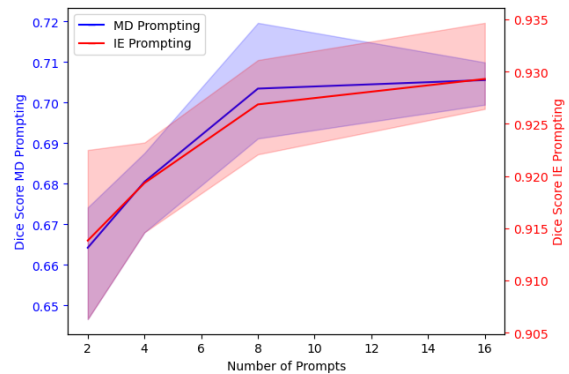


Figure 5. Ablation: investigating the effect of different numbers of prompts in mask decoder (MD) and image encoder (IE). For the blue MD curve, the image encoder is frozen, meaning  $n_{ie} = 0$ . For the red IE curve, we use  $n_{md} = 8$ . Note the two y-axes scales.

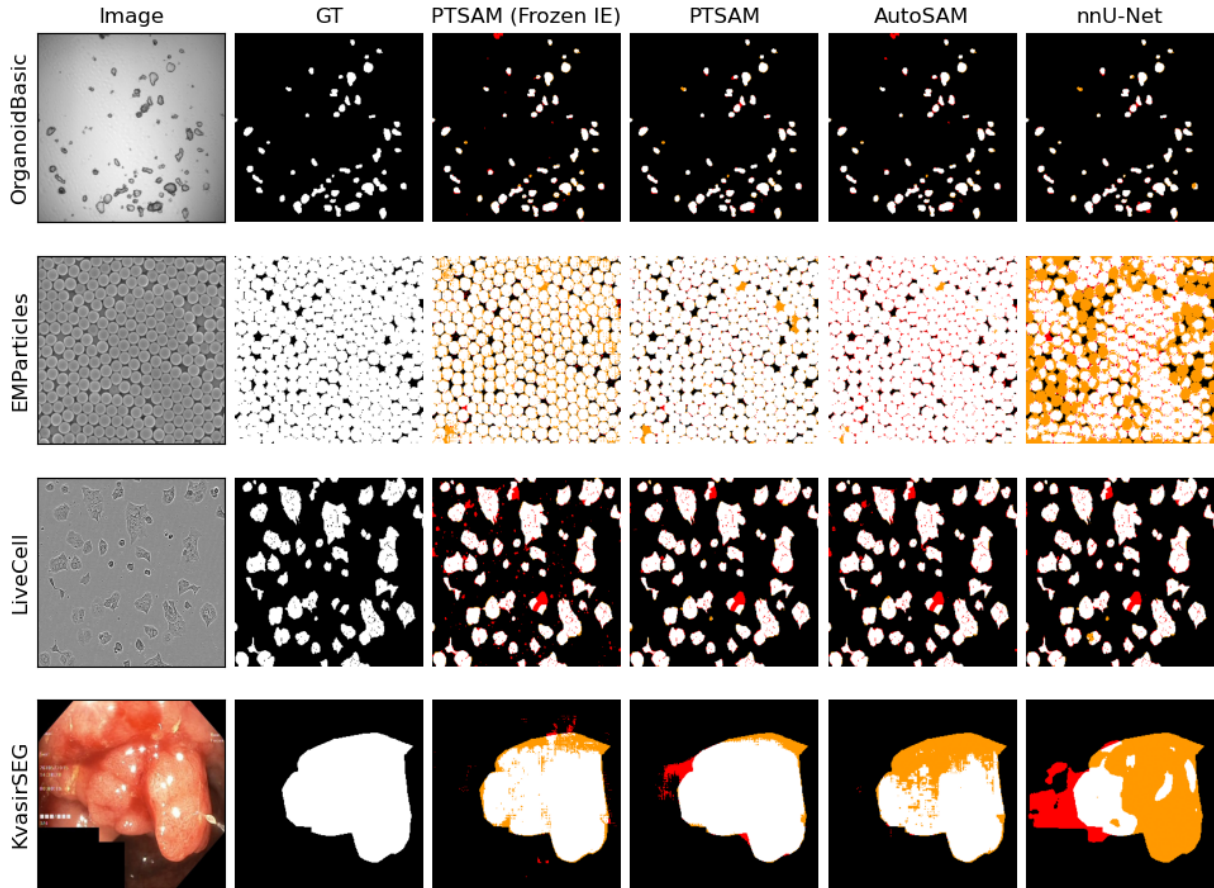


Figure 6. Qualitative segmentation results on three microscopy and one medical dataset (top to bottom). On each dataset, one example image along with its ground truth annotation as well as segmentation results of four chosen methods are shown from left to right. Results were obtained with models trained in a few-shot scenario with only 16 training samples. See Sec. 4.2.5 for details. Red areas indicate a false positive segmentation, whereas orange indicates false negatives.

the image encoder with varying numbers of prompts. Similar to the number of mask decoder prompts, inserting more than 8 tokens only shows diminishing returns.

## 5. Conclusion

We presented prompt-tuning SAM (PTSAM), a novel method for training a semantic segmentation model for data-limited non-natural image domains such as microscopy or medical image analysis. PTSAM builds upon the strong segmentation capabilities of Segment Anything (SAM) and leverages prompt-tuning to adapt SAM to a new task and a new domain in a data-efficient and parameter-efficient manner. Our approach solves two common problems of SAM for specialized applications: the necessity for spatial prompting for semantic mask generation, and the performance decrease under domain shifts.

We evaluated PTSAM on three microscopic and one medical dataset and compared it with three state-of-the-art

methods for adapting SAM as well as nnU-Net as the de-facto standard for semantic segmentation tasks. We found that turning SAM from a generalist into a use-case specialist model only requires 2,048 parameters, while providing segmentation accuracy on-par with methods requiring  $> 10\times$  more parameters to adapt. We observed that this parameter efficiency makes PTSAM robust to overfitting, which allows for additionally adapting the image encoder with as few as 16 training samples. While we found the segmentation accuracy of other methods decreasing when additionally adapting the image encoder, PTSAM’s accuracy did not only not decrease but even increased further, even in such few-shot data-limited applications. In summary, we can conclude that PTSAM is an attractive combination of parameter efficiency and resulting segmentation accuracy for applications with limited training data and domain shifts. We therefore see PTSAM an out-of-the-box solution for domain-specific image segmentation tasks, requiring only few annotated samples and no hyperparameters to tune.



## References

- [1] Josh Achiam et al. GPT-4 technical report. *arXiv preprint arXiv:2303.08774*, 2023. 1, 2
- [2] Sidra Akbar, Shahzad Nasim, Sarwar Wasi, and Syed Muhammad Ussama Zafar. Image analysis for mri based brain tumor detection. *2019 4th International Conference on Emerging Trends in Engineering, Sciences and Technology (ICEEST)*, pages 1–5, 2019. 1
- [3] Asaad Anaam, Mugahed A. Al-antari, Jamil Hussain, Naganwan Abdel Samee, Maali Alabdulhafith, and Akio Gofuku. Deep active learning for automatic mitotic cell detection on hep-2 specimen medical images. *Diagnostics*, 13, 2023. 1
- [4] Anwai Archit, Luca Freckmann, Sushmita Nair, Nabeel Khalid, Paul Hilt, Vikas Rajashekar, Marei Freitag, Carolin Teuber, Genevieve Buckley, Sebastian von Haaren, et al. Segment anything for microscopy. *Nature Methods*, pages 1–13, 2025. 2, 3
- [5] Samyadeep Basu, Shell Xu Hu, Daniela Massiceti, and Soheil Feizi. Strong baselines for parameter-efficient few-shot fine-tuning. In *Thirty-Eighth AAAI Conference on Artificial Intelligence, AAAI 2024, Thirty-Sixth Conference on Innovative Applications of Artificial Intelligence, IAAI 2024, Fourteenth Symposium on Educational Advances in Artificial Intelligence, EAAI 2024, February 20-27, 2024, Vancouver, Canada*, pages 11024–11031. AAAI Press, 2024. 2
- [6] Rishi Bommasani, Drew A. Hudson, Ehsan Adeli, et al. On the opportunities and risks of foundation models. *ArXiv preprint*, abs/2108.07258, 2021. 1, 2
- [7] Tom B. Brown, Benjamin Mann, Nick Ryder, et al. Language models are few-shot learners. In *Advances in Neural Information Processing Systems 33: Annual Conference on Neural Information Processing Systems 2020, NeurIPS 2020, December 6-12, 2020, virtual*, 2020. 1, 2
- [8] Victor Ion Butoi, Jose Javier Gonzalez Ortiz, Tianyu Ma, Mert Rory Sabuncu, John V. Guttag, and Adrian V. Dalca. Universeg: Universal medical image segmentation. *2023 IEEE/CVF International Conference on Computer Vision (ICCV)*, pages 21381–21394, 2023. 2
- [9] Han Cai, Chuang Gan, Ligeng Zhu, and Song Han. Tinytl: Reduce activations, not trainable parameters for efficient on-device learning. *ArXiv preprint*, abs/2007.11622, 2020. 2
- [10] Ruining Deng, Can Cui, Quan Liu, Tianyuan Yao, Lucas W Remedios, Shunxing Bao, Bennett A Landman, Lee E Wheless, Lori A Coburn, Keith T Wilson, et al. Segment anything model (sam) for digital pathology: Assess zero-shot segmentation on whole slide imaging. *ArXiv preprint*, abs/2304.04155, 2023. 2
- [11] Tim Dettmers, Artidoro Pagnoni, Ari Holtzman, and Luke Zettlemoyer. Qlora: Efficient finetuning of quantized llms. In *Advances in Neural Information Processing Systems 36: Annual Conference on Neural Information Processing Systems 2023, NeurIPS 2023, New Orleans, LA, USA, December 10 - 16, 2023*, 2023. 3
- [12] Jeff Donahue, Yangqing Jia, Oriol Vinyals, Judy Hoffman, Ning Zhang, Eric Tzeng, and Trevor Darrell. Decaf: A deep convolutional activation feature for generic visual recognition. In *Proceedings of the 31th International Conference on Machine Learning, ICML 2014, Beijing, China, 21-26 June 2014*, pages 647–655. JMLR.org, 2014. 2
- [13] Alexey Dosovitskiy, Lucas Beyer, Alexander Kolesnikov, Dirk Weissenborn, Xiaohua Zhai, Thomas Unterthiner, Mostafa Dehghani, Matthias Minderer, Georg Heigold, Sylvain Gelly, Jakob Uszkoreit, and Neil Houlsby. An image is worth 16x16 words: Transformers for image recognition at scale. In *9th International Conference on Learning Representations, ICLR 2021, Virtual Event, Austria, May 3-7, 2021*. OpenReview.net, 2021. 2, 3
- [14] Christoffer Edlund, Timothy R. Jackson, Nabeel Khalid, Nicola J Bevan, Timothy Dale, Andreas R. Dengel, Sheraz Ahmed, Johan Trygg, and Rickard Sjögren. Livecell—a large-scale dataset for label-free live cell segmentation. *Nature Methods*, 18:1038 – 1045, 2021. 5
- [15] Zeyu Han, Chao Gao, Jinyang Liu, Jeff Zhang, and Sai Qian Zhang. Parameter-efficient fine-tuning for large models: A comprehensive survey. *ArXiv preprint*, abs/2403.14608, 2024. 2
- [16] Ali Hatamizadeh, Vishwesh Nath, Yucheng Tang, Dong Yang, Holger R Roth, and Daguang Xu. Swin unetr: Swin transformers for semantic segmentation of brain tumors in mri images. In *International MICCAI brainlesion workshop*, pages 272–284. Springer, 2021. 2
- [17] Ali Hatamizadeh, Yucheng Tang, Vishwesh Nath, Dong Yang, Andriy Myronenko, Bennett Landman, Holger Roth, and Daguang Xu. UNETR: Transformers for 3d medical image segmentation, 2021. 3
- [18] Ali Hatamizadeh, Yucheng Tang, Vishwesh Nath, Dong Yang, Andriy Myronenko, Bennett Landman, Holger R Roth, and Daguang Xu. Unetr: Transformers for 3d medical image segmentation. In *Proceedings of the IEEE/CVF winter conference on applications of computer vision*, pages 574–584, 2022. 2
- [19] Kaiming He, Xiangyu Zhang, Shaoqing Ren, and Jian Sun. Deep residual learning for image recognition. In *Proceedings of the IEEE conference on computer vision and pattern recognition*, pages 770–778, 2016. 2
- [20] Kaiming He, Georgia Gkioxari, Piotr Dollár, and Ross B. Girshick. Mask R-CNN. In *IEEE International Conference on Computer Vision, ICCV 2017, Venice, Italy, October 22-29, 2017*, pages 2980–2988. IEEE Computer Society, 2017. 2
- [21] Kaiming He, Xinlei Chen, Saining Xie, Yanghao Li, Piotr Dollár, and Ross B. Girshick. Masked autoencoders are scalable vision learners. In *IEEE/CVF Conference on Computer Vision and Pattern Recognition, CVPR 2022, New Orleans, LA, USA, June 18-24, 2022*, pages 15979–15988. IEEE, 2022. 2, 3
- [22] Neil Houlsby, Andrei Giurgiu, Stanislaw Jastrzebski, Bruna Morrone, Quentin de Laroussilhe, Andrea Gesmundo, Mona Attariyan, and Sylvain Gelly. Parameter-efficient transfer learning for NLP. In *Proceedings of the 36th International Conference on Machine Learning, ICML 2019, 9-15 June 2019, Long Beach, California, USA*, pages 2790–2799. PMLR, 2019. 2

- [23] Jeremy Howard and Sebastian Ruder. Universal language model fine-tuning for text classification. In *Proceedings of the 56th Annual Meeting of the Association for Computational Linguistics (Volume 1: Long Papers)*, pages 328–339, Melbourne, Australia, 2018. Association for Computational Linguistics. 2
- [24] Edward J. Hu, Yelong Shen, Phillip Wallis, Zeyuan Allen-Zhu, Yanzhi Li, Shean Wang, Lu Wang, and Weizhu Chen. Lora: Low-rank adaptation of large language models. In *The Tenth International Conference on Learning Representations, ICLR 2022, Virtual Event, April 25-29, 2022*. OpenReview.net, 2022. 3, 4
- [25] Xinrong Hu, Xiaowei Xu, and Yiyu Shi. How to efficiently adapt large segmentation model(sam) to medical images, 2023. 3, 5, 6
- [26] Fabian Isensee, Jens Petersen, André Klein, David Zimmerer, P. Jaeger, Simon A. A. Kohl, J. Wasserthal, Gregor Koehler, T. Norajitra, Sebastian J. Wirkert, and Klaus Hermann Maier-Hein. nnu-net: Self-adapting framework for u-net-based medical image segmentation. *ArXiv preprint*, abs/1809.10486, 2018. 2, 5
- [27] Uriah Israel, Markus Marks, Rohit Dilip, Qilin Li, Morgan Schwartz, Elora Pradhan, Edward Pao, Shenyi Li, Alexander Pearson-Goulart, Pietro Perona, Georgia Gkioxari, Ross Barnowski, Yisong Yue, and David Van Valen. A foundation model for cell segmentation, 2023. 2, 3, 5
- [28] Debesh Jha, Pia Helen Smedsrud, M. Riegler, P. Halvorsen, Thomas de Lange, Dag Johansen, and Haavard D. Johansen. Kvasir-seg: A segmented polyp dataset. In *Conference on Multimedia Modeling*, 2019. 5
- [29] Wei Ji, Jingjing Li, Qi Bi, Tingwei Liu, Wenbo Li, and Li Cheng. Segment anything is not always perfect: An investigation of sam on different real-world applications, 2024. 2
- [30] Menglin Jia, Luming Tang, Bor-Chun Chen, Claire Cardie, Serge J. Belongie, Bharath Hariharan, and Ser Nam Lim. Visual prompt tuning. *ArXiv preprint*, abs/2203.12119, 2022. 2, 3, 4
- [31] Alexander Kirillov, Eric Mintun, Nikhila Ravi, Hanzi Mao, Chloé Rolland, Laura Gustafson, Tete Xiao, Spencer Whitehead, Alexander C. Berg, Wan-Yen Lo, Piotr Dollár, and Ross B. Girshick. Segment anything. In *IEEE/CVF International Conference on Computer Vision, ICCV 2023, Paris, France, October 1-6, 2023*, pages 3992–4003. IEEE, 2023. 2, 3
- [32] Michael Y. Lee, Jacob S. Bedia, Salil S. Bhate, Graham L. Barlow, Darci Phillips, Wendy J. Fantl, Garry P. Nolan, and Christian M. Schürch. Cellseg: a robust, pre-trained nucleus segmentation and pixel quantification software for highly multiplexed fluorescence images. *BMC Bioinformatics*, 23, 2022. 2
- [33] Juliet Lefferts, Suzanne Kroes, Matthew B Smith, Paul J Niemöller, Natascha D A Nieuwenhuijze, Heleen N Sonneveld van Kooten, Cornelis K. van der Ent, Jeffrey M. Beekman, and Sam F B van Beuningen. Orgasegment: deep-learning based organoid segmentation to quantify cfr dependent fluid secretion. *Communications Biology*, 7, 2024. 5
- [34] Brian Lester, Rami Al-Rfou, and Noah Constant. The power of scale for parameter-efficient prompt tuning. In *Proceedings of the 2021 Conference on Empirical Methods in Natural Language Processing*, pages 3045–3059, Online and Punta Cana, Dominican Republic, 2021. Association for Computational Linguistics. 2
- [35] Kevin Li and Pranav Rajpurkar. Adapting segment anything models to medical imaging via fine-tuning without domain pretraining. In *AAAI 2024 Spring Symposium on Clinical Foundation Models*, 2024. 5
- [36] Xiang Lisa Li and Percy Liang. Prefix-tuning: Optimizing continuous prompts for generation. In *Proceedings of the 59th Annual Meeting of the Association for Computational Linguistics and the 11th International Joint Conference on Natural Language Processing (Volume 1: Long Papers)*, pages 4582–4597, Online, 2021. Association for Computational Linguistics. 2
- [37] Yanghao Li, Hanzi Mao, Ross Girshick, and Kaiming He. Exploring plain vision transformer backbones for object detection. In *European conference on computer vision*, pages 280–296. Springer, 2022. 4
- [38] Zhaojiang Lin, Andrea Madotto, and Pascale Fung. Exploring versatile generative language model via parameter-efficient transfer learning. In *Findings of the Association for Computational Linguistics: EMNLP 2020*, pages 441–459, Online, 2020. Association for Computational Linguistics. 2
- [39] Jonathan Long, Evan Shelhamer, and Trevor Darrell. Fully convolutional networks for semantic segmentation. In *IEEE Conference on Computer Vision and Pattern Recognition, CVPR 2015, Boston, MA, USA, June 7-12, 2015*, pages 3431–3440. IEEE Computer Society, 2015. 2
- [40] Ilya Loshchilov and Frank Hutter. SGDR: stochastic gradient descent with warm restarts. In *5th International Conference on Learning Representations, ICLR 2017, Toulon, France, April 24-26, 2017, Conference Track Proceedings*. OpenReview.net, 2017. 5
- [41] Ilya Loshchilov and Frank Hutter. Decoupled weight decay regularization. In *7th International Conference on Learning Representations, ICLR 2019, New Orleans, LA, USA, May 6-9, 2019*. OpenReview.net, 2019. 5
- [42] Jun Ma, Yuting He, Feifei Li, Lin Han, Chenyu You, and Bo Wang. Segment anything in medical images, 2023. 5, 6
- [43] Saiyang Na, Yuzhi Guo, Feng Jiang, Hehuan Ma, and Junzhou Huang. Segment any cell: A sam-based auto-prompting fine-tuning framework for nuclei segmentation. *ArXiv preprint*, abs/2401.13220, 2024. 2, 3
- [44] Laurentino Biccias Neto and Caio Regattieri. Retfound: Training robust medical imaging-based diagnostic models via self-supervised learning. *Arquivos Brasileiros de Oftalmologia*, 2023. 2
- [45] Alec Radford, Jong Wook Kim, Chris Hallacy, Aditya Ramesh, Gabriel Goh, Sandhini Agarwal, Girish Sastry, Amanda Askell, Pamela Mishkin, Jack Clark, Gretchen Krueger, and Ilya Sutskever. Learning transferable visual models from natural language supervision. In *Proceedings of the 38th International Conference on Machine Learning, ICML 2021, 18-24 July 2021, Virtual Event*, pages 8748–8763. PMLR, 2021. 2
- [46] Olaf Ronneberger, Philipp Fischer, and Thomas Brox. U-net:

- Convolutional networks for biomedical image segmentation. *ArXiv preprint*, abs/1505.04597, 2015. 2, 3
- [47] Andreas Rücklé, Gregor Geigle, Max Glockner, Tilman Beck, Jonas Pfeiffer, Nils Reimers, and Iryna Gurevych. AdapterDrop: On the efficiency of adapters in transformers. In *Proceedings of the 2021 Conference on Empirical Methods in Natural Language Processing*, pages 7930–7946, Online and Punta Cana, Dominican Republic, 2021. Association for Computational Linguistics. 2
- [48] Julian Schröter, Luca Deininger, Blaz Lupse, Petra Richter, Steffen Syrbe, Ralf Mikut, and Sabine Jung-Klawitter. A large and diverse brain organoid dataset of 1,400 cross-laboratory images of 64 trackable brain organoids. *Scientific Data*, 11, 2024. 1
- [49] Qian Shen, Zhuoshi Li, Yuanyuan Chen, Haojie Gu, Qian Chen, and Chao Zuo. Cell segmentation and dry mass characterization based on slightly off-axis holographic imaging. In *International Conference on Optical and Photonic Engineering*, 2023. 1
- [50] Neeru Singla, Ajay Kumar, Himanshu Rikhari, and Vishal Srivastava. A review paper on microscopic modalities used in biomedical applications. In *European Journal of Molecular & Clinical Medicine*, 2020. 1
- [51] Hugo Touvron, Matthieu Cord, Alaaeldin El-Nouby, Jakob Verbeek, and Hervé Jégou. Three things everyone should know about vision transformers. In *European Conference on Computer Vision*, pages 497–515. Springer, 2022. 2
- [52] Illia Tsiporenko, Pavel Chizhov, and Dmytro Fishman. Going beyond u-net: Assessing vision transformers for semantic segmentation in microscopy image analysis. *ArXiv preprint*, abs/2409.16940, 2024. 2
- [53] Sam F. B. van Beuningen, Juliet Lefferts, and University Medical Center Utrecht. Organoid basic, 2023. 5
- [54] Alexandra D. VandeLoo, Nathan J. Malta, Emilio Aponte, Caitlin van Zyl, Danfei Xu, and Craig R. Forest. Samcell: Generalized label-free biological cell segmentation with segment anything. *bioRxiv*, 2025. 2, 3, 4, 5
- [55] Ashish Vaswani, Noam Shazeer, Niki Parmar, Jakob Uszkoreit, Llion Jones, Aidan N. Gomez, Lukasz Kaiser, and Illia Polosukhin. Attention is all you need. In *Advances in Neural Information Processing Systems 30: Annual Conference on Neural Information Processing Systems 2017, December 4-9, 2017, Long Beach, CA, USA*, pages 5998–6008, 2017. 1, 2
- [56] Yingming Wang, Xiangyu Zhang, Tong Yang, and Jian Sun. Anchor DETR: query design for transformer-based detector. In *Thirty-Sixth AAAI Conference on Artificial Intelligence, AAAI 2022, Thirty-Fourth Conference on Innovative Applications of Artificial Intelligence, IAAI 2022, The Twelveth Symposium on Educational Advances in Artificial Intelligence, EAAI 2022 Virtual Event, February 22 - March 1, 2022*, pages 2567–2575. AAAI Press, 2022. 3
- [57] Qi Wu, Yuyao Zhang, and Marawan Elbatel. Self-prompting large vision models for few-shot medical image segmentation, 2023. 3
- [58] Yi Xin, Siqi Luo, Haodi Zhou, Junlong Du, Xiaohong Liu, Yue Fan, Qing Li, and Yuntao Du. Parameter-efficient fine-tuning for pre-trained vision models: A survey. *ArXiv preprint*, abs/2402.02242, 2024. 2
- [59] Lingling Xu, Haoran Xie, S. Joe Qin, Xiaohui Tao, and Fu Lee Wang. Parameter-efficient fine-tuning methods for pretrained language models: A critical review and assessment. *ArXiv preprint*, abs/2312.12148, 2023. 2
- [60] Lihe Yang, Bingyi Kang, Zilong Huang, Xiaogang Xu, Jiashi Feng, and Hengshuang Zhao. Depth anything: Unleashing the power of large-scale unlabeled data. *2024 IEEE/CVF Conference on Computer Vision and Pattern Recognition (CVPR)*, pages 10371–10381, 2024. 2
- [61] Batuhan Yildirim and Jacqueline M. Cole. Bayesian particle instance segmentation for electron microscopy image quantification. *Journal of Chemical Information and Modeling*, 61(3):1136–1149, 2021. PMID: 33682402. 5
- [62] Kaidong Zhang and Dong Liu. Customized segment anything model for medical image segmentation, 2023. 3, 4, 5
- [63] Sixiao Zheng, Jiachen Lu, Hengshuang Zhao, Xiatian Zhu, Zekun Luo, Yabiao Wang, Yanwei Fu, Jianfeng Feng, Tao Xiang, Philip H. S. Torr, and Li Zhang. Rethinking semantic segmentation from a sequence-to-sequence perspective with transformers. In *IEEE Conference on Computer Vision and Pattern Recognition, CVPR 2021, virtual, June 19-25, 2021*, pages 6881–6890. Computer Vision Foundation / IEEE, 2021. 2
- [64] Peilin Zhou, Bo Du, and Yongchao Xu. Cellseg1: Robust cell segmentation with one training image, 2024. 3, 4, 5